Correspondence

Effect of Mutual Coupling on the Channel Capacity of MIMO Systems

Kuan-Hao Chen and Jean-Fu Kiang

***Abstract*—The reciprocity theorem is applied to derive an exact expression that is used to remove the coupling effects embedded in the receiving voltages of an antenna array. The correlation coefficients of the multiple-input–multiple-output (MIMO) channel established with the antenna array is also modified to incorporate the direction-dependent coupling effects more accurately. The effects of mutual coupling on the channel capacity of MIMO systems in a line-of-sight (LOS), as well as a multipath environments, under different coupling assumptions, are simulated and compared.**

***Index Terms*—Channel capacity, multiple-input–multiple-output (MIMO), mutual coupling, phased arrays.**

I. Introduction

Multiple-input–multiple-output (MIMO) antennas have been proposed to increase the channel capacity of wireless systems in an environment filled with rich multipath signals [1], [2]. In modeling a MIMO channel, it is generally assumed that the coefficients of the channel transfer matrix are independent and identically distributed. When the antennas are placed close to one another or when there are fewer scatterers in between the transmitting and the receiving arrays, the correlation coefficients will increase; hence, the channel capacity will be reduced [3].

At smaller antenna spacing, the variation of mutual coupling among antennas will affect the channel capacity more significantly. It was reported that mutual coupling may increase the channel capacity by decreasing the spatial correlation coefficients under certain circumferences [4]. In [5], a network theory was used to derive the transfer matrix, which includes the coupling effects among antennas in both the transmitting and the receiving arrays, the multipath propagation channel, the receiver matching network, and the noise in the receiver amplifiers.

The spatial covariance matrix, which is critical to model a MIMO channel, is determined by the power angular spectrum (PAS) and the radiation patterns of the antennas [6], [7]. In a wireless system where the MIMO antennas are closely placed to one another, the radiation pattern of each antenna will be distorted from its original design, leading to the reduction of space diversity and pattern diversity. The coupling effect should be incorporated in calculating the correlation coefficients.

Other techniques have also been proposed to increase the pattern diversity, including the use of a compact broadband MIMO antenna with separate antennas operating at independent modes to provide multimode diversity [8], the use of an antenna supporting orthogonal modes to achieve pattern orthogonality [9], and the reduction of the correlation among MIMO antennas by inserting parasitic elements to reduce mutual coupling [10].

In this paper, we derive a relation between the receiving voltages and the open-circuit voltages at antennas of an array, based on the reciprocity theorem. The channel capacity of MIMO channels is simulated under different coupling assumptions, to study the significance of mutual coupling effects in different propagation environments. This paper is organized as follows. The MIMO channel modeling is briefly reviewed in Section II. The effect of mutual coupling on the correlation coefficients is presented in Section III. The capacity with a water-filling power distribution strategy, including mutual coupling effects, is presented in Section IV. Simulation results are presented in Section V. Finally, some conclusions are drawn in Section VI.

II. Multiple-Input–Multiple-Output Channel Modeling

A typical MIMO channel, which is composed of N_t transmitting antennas and N_r receiving antennas, can be described as [11]

$$\bar{y} = \bar{\bar{H}} \cdot \bar{x} + \bar{n} \tag{1}$$

where $\bar{y}$ contains N_r received signals, $\bar{x}$ contains N_t transmitted signals, $\bar{\bar{H}}$ is the channel transfer matrix of dimension $N_r \times N_t$, and $\bar{n}$ contains N_r independent Gaussian-distributed noise of variance σ_n^2.

If the transmitted signals $\bar{x}$ are modeled as complex Gaussian random variables, the channel capacity can be expressed as [11]

$$C = \max_{\bar{\bar{R}}_{xx}:\mathrm{Tr}\{\bar{\bar{R}}_{xx}\}\le P_t} \log_2 \det\left\{\bar{\bar{I}} + \frac{\bar{\bar{H}} \cdot \bar{\bar{R}}_{xx} \cdot \bar{\bar{H}}^\dagger}{\sigma_n^2}\right\} \tag{2}$$

where $\bar{\bar{I}}$ is an $N_r \times N_r$ identity matrix, $\mathrm{Tr}\{\bar{\bar{A}}\}$ is the trace of $\bar{\bar{A}}$, and P_t is the total transmitting power. The diagonal elements of the covariance matrix $\bar{\bar{R}}_{xx} = \mathrm{E}\{\bar{x}\bar{x}^\dagger\}$ represent the transmitting power from each antenna, and the constraint $\mathrm{Tr}\{\bar{\bar{R}}_{xx}\} \le P_t$ means the total transmitting power cannot be larger than P_t.

Without prior information on $\bar{\bar{H}}$, it is reasonable to allocate the transmitting power evenly among all the transmitting antennas, namely, $\bar{\bar{R}}_{xx} = (P_t/N_t)\bar{\bar{I}}$. The transmitting capacity is thus obtained as [1]

$$C_U = \log_2 \det\left\{\bar{\bar{I}} + \frac{P_t}{N_t\sigma_n^2}\bar{\bar{H}} \cdot \bar{\bar{H}}^\dagger\right\}. \tag{3}$$

The transfer matrix $\bar{\bar{H}}$ is often characterized with statistical terms. Over a non-line-of-sight (NLOS) channel between two antennas, the amplitude and phase responses can be fairly described with a Rayleigh distribution and a uniform distribution, respectively [12]. Thus, the channel can be completely specified with $\bar{R} = \mathrm{E}\{\bar{h}\bar{h}^\dagger\}$, where $\bar{h} = \mathrm{vec}\{\bar{\bar{H}}\}$ is formed by stacking all columns of $\bar{\bar{H}}$.

Assuming that the link between a single transmitting antenna and a single receiving antenna is independent of another link, the covariance matrix of the channel can be expressed as $\bar{\bar{R}} = \bar{\bar{R}}_t \otimes \bar{\bar{R}}_r$ [13], where $\bar{\bar{R}}_t$ and $\bar{\bar{R}}_r$ are the covariance matrices of the transmitting and the receiving arrays, respectively, and $\otimes$ represents a Kronecker product. Thus, the transfer matrix $\bar{\bar{H}}$ can be reduced to [14]

$$\bar{\bar{H}} = \bar{\bar{R}}_r^{\frac{1}{2}} \cdot \bar{\bar{H}}_{\mathrm{i.i.d.}} \cdot \bar{\bar{R}}_t^{\frac{1}{2}} \tag{4}$$

Manuscript received August 7, 2014; revised December 13, 2014, January 15, 2015, and January 20, 2015; accepted January 25, 2015. Date of publication January 27, 2015; date of current version January 13, 2016. This work was supported in part by the Taiwan Ministry of Science and Technology under Contract NSC102-2221-E-002-043. The review of this paper was coordinated by Dr. N.-D. Dao.

The authors are with the Department of Electrical Engineering and the Graduate Institute of Communication Engineering, National Taiwan University, Taipei 106, Taiwan (e-mail: jfkiang@ntu.edu.tw).

Digital Object Identifier 10.1109/TVT.2015.2397033

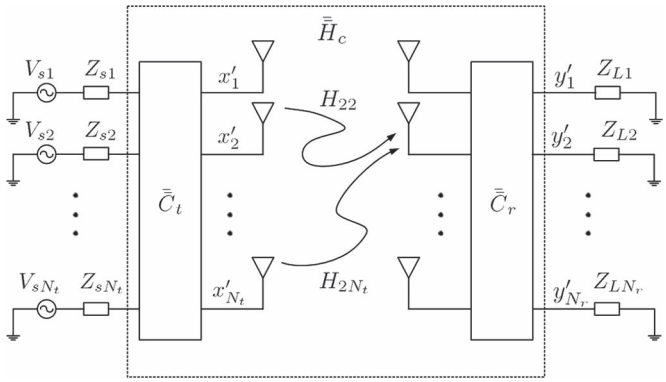

Fig. 1. $N_t \times N_r$ MIMO channel, with mutual coupling among antennas in the same array.

where $\bar{\bar{H}}_{\text{i.i.d.}}$ is an $N_r \times N_t$ matrix of independent and identically distributed (i.i.d.) complex Gaussian random variables, each with zero mean and unit variance.

The average MIMO channel capacity (in bits per second per Hertz), with the strategy of uniformly distributed transmitting power, can be determined as [15]

$$C_U = \mathrm{E}\left\{\log_2 \det\left[\bar{\bar{I}} + \frac{\mathrm{SNR}}{N_t}\bar{\bar{H}} \cdot \bar{\bar{H}}^{\dagger}\right]\right\} \tag{5}$$

where $\mathrm{SNR} = P_t/\sigma_n^2$ is the signal-to-noise ratio, and the expectation value is taken over all possible channel conditions described by $\bar{\bar{H}}$.

A. Mutual Coupling

Fig. 1 shows an $N_t \times N_r$ MIMO channel, with mutual coupling among antennas in the same array. The transmitted signals can thus be expressed as

$$\bar{x}' = \bar{\bar{C}}_t \cdot \bar{x} \tag{6}$$

where $\bar{\bar{C}}_t = (\bar{\bar{Z}}_s + \bar{\bar{Z}}_{\text{ant}}) \cdot (\bar{\bar{Z}}_t + \bar{\bar{Z}}_s)^{-1}$ is the coupling matrix of the transmitting array, $\bar{\bar{Z}}_t$, $\bar{\bar{Z}}_s$, and $\bar{\bar{Z}}_{\text{ant}}$ are the mutual impedance matrix, source impedance, and antenna input impedance, respectively, of the transmitting array [16].

Similarly, the receiving signals under the mutual coupling effect can be expressed as

$$\bar{y}' = \bar{\bar{C}}_r \cdot \bar{\bar{H}} \cdot \bar{x}' + \bar{n} = \bar{\bar{C}}_r \cdot \bar{\bar{H}} \cdot \bar{\bar{C}}_t \cdot \bar{x} + \bar{n} = \bar{\bar{H}}_c \cdot \bar{x} + \bar{n} \tag{7}$$

where $\bar{\bar{H}}_c$ is the transfer matrix including the mutual coupling effects [17], and $\bar{\bar{C}}_r$ is the coupling matrix of the receiving array [18].

B. Covariance Matrices

The covariance matrices $\bar{\bar{R}}_t$ and $\bar{\bar{R}}_r$ have the explicit forms of

$$\bar{\bar{R}}_t = \begin{bmatrix} 1 & \rho_{t,12} & \cdots & \rho_{t,1N_t} \\ \rho_{t,21} & 1 & \cdots & \rho_{t,2N_t} \\ \vdots & \vdots & \ddots & \vdots \\ \rho_{t,N_t1} & \rho_{t,N_t2} & \cdots & 1 \end{bmatrix}_{N_t \times N_t}$$

$$\bar{\bar{R}}_r = \begin{bmatrix} 1 & \rho_{r,12} & \cdots & \rho_{r,1N_r} \\ \rho_{r,21} & 1 & \cdots & \rho_{r,2N_r} \\ \vdots & \vdots & \ddots & \vdots \\ \rho_{r,N_r1} & \rho_{r,N_r2} & \cdots & 1 \end{bmatrix}_{N_r \times N_r}$$

where $\rho_{t,mn}$ and $\rho_{r,mn}$ are the correlation coefficients in the transmitting array and the receiving array, respectively, which can be computed as [6]

$$\rho_{mn} = \frac{1}{\sigma_m \sigma_n} \int_0^{\pi} d\theta \int_{-\pi}^{\pi} d\phi \sin\theta \left[\chi p_\theta(\theta,\phi) E_{m\theta}(\theta,\phi) \times E^*_{n\theta}(\theta,\phi) + p_\phi(\theta,\phi) E_{m\phi}(\theta,\phi) E^*_{n\phi}(\theta,\phi)\right] \tag{8}$$

where $E_{\ell\theta}(\theta,\phi)$ and $E_{\ell\phi}(\theta,\phi)$ are the θ and ϕ components, respectively, of the far-field radiated by the ℓth antenna

$$\sigma_\ell^2 = \int_0^{\pi} d\theta \int_{-\pi}^{\pi} d\phi \sin\theta \left[\chi p_\theta(\theta,\phi) |E_{\ell\theta}(\theta,\phi)|^2 + p_\phi(\theta,\phi) |E_{\ell\phi}(\theta,\phi)|^2\right]$$

$p_\theta(\theta,\phi)$ and $p_\phi(\theta,\phi)$ are the PASs, and $\chi = P_v/P_h$ is the cross-polarization ratio, with

$$P_v = \int_{-\pi}^{\pi} d\phi \int_0^{\pi} d\theta \sin\theta \, |E_{i\theta}(\theta,\phi)|^2$$

$$P_h = \int_{-\pi}^{\pi} d\phi \int_0^{\pi} d\theta \sin\theta \, |E_{i\phi}(\theta,\phi)|^2$$

where $E_{i\theta}(\theta,\phi)$ and $E_{i\phi}(\theta,\phi)$ are the incident fields.

In a typical wireless environment, incident waves can be attributed to several clusters over the angular domain, each is commonly modeled by a uniform, a truncated Gaussian, or a truncated Laplacian PAS [7].

III. Mutual Coupling Effects on Correlation Coefficients

As shown in (7), the effects of mutual coupling on the transfer matrix $\bar{\bar{H}}$ is accounted for with the coupling matrices $\bar{\bar{C}}_t$ and $\bar{\bar{C}}_r$. To calculate the correlation coefficients in (8), the radiation pattern $E_\ell(\theta,\phi)$ is approximated as that of an isolated antenna.

By applying the reciprocity theorem, the receiving voltages and the open-circuit voltages at the input ports of the receiving antennas are related as

$$\begin{aligned} \bar{V}_r(\theta_i,\phi_i) &= \bar{\bar{Z}}^{-1} \cdot \left[\bar{\bar{A}} \cdot \bar{V}_{\text{oc}}(\theta_i,\phi_i) - \bar{\bar{G}} \cdot \bar{E}(\theta_i,\phi_i)\right] \\ &= \bar{\bar{B}} \cdot \bar{V}_{\text{oc}}(\theta_i,\phi_i) + \bar{D}(\theta_i,\phi_i) \end{aligned} \tag{9}$$

where $\bar{\bar{B}} = \bar{\bar{Z}}^{-1} \cdot \bar{\bar{A}}$; $\bar{D}(\theta_i,\phi_i) = -\bar{\bar{Z}}^{-1} \cdot \bar{\bar{G}}(\theta_i) \cdot \bar{E}(\theta_i,\phi_i)$

$$Z_{mn} = \begin{cases} \frac{V_{sm}}{Z_{Lm} I_{t,mm}(0)}, & m = n \\ 0, & m \neq n \end{cases}$$

$$G_{mn}(\theta_i) = \begin{cases} \frac{1}{I_{t,mm}(0)} \int_{-L_m/2}^{\frac{L_m}{2}} I_{t,mc}(z') e^{jkz'\cos\theta_i} dz', & m = n \\ \frac{1}{I_{t,mm}(0)} \int_{-L_n/2}^{\frac{L_n}{2}} I_{t,nm}(z') e^{jkz'\cos\theta_i} dz', & m \neq n \end{cases}$$

$$A_{mn} = \begin{cases} \frac{I_t(0)}{I_{t,mm}(0)}, & m = n \\ 0, & m \neq n \end{cases}$$

$$E_n(\theta_i,\phi_i) = E_0 e^{jk\left(x'_n \sin\theta_i \cos\phi_i + y'_n \sin\theta_i \sin\phi_i\right)}$$

$$V_{\mathrm{oc}m}(\theta_i,\phi_i) = -\frac{1}{I_t(0)} E_0 e^{jk\left(x'_m \sin\theta_i \cos\phi_i + y'_m \sin\theta_i \sin\phi_i\right)} \times \int_{-L_m/2}^{\frac{L_m}{2}} dz' I_t(z') e^{jkz' \cos\theta_i}$$

with $1 \le m, n \le N_r$; V_{sm} is the source voltage of the mth antenna in the transmitting mode; Z_{Lm} is the load impedance of the mth antenna, which is assumed conjugate matched to its input impedance; I_t is the current distribution on an isolated antenna; $I_{t,mm}$ is the transmitting current in the absence of the other antennas; $I_{t,mc}$ is the current coupled from the other antennas to the mth antenna; and $I_{t,nm}$ is the induced current on the nth antenna due to the mth antenna.

To focus on the coupling effects on the channel capacity, while keeping the simulation scenarios simple, we place both the transmitting array and the receiving array on the xy-plane, and assume that the signals are incident at $\theta_{\mathrm{in}} = 90^\circ$. Thus, the receiving correlation coefficients, including mutual coupling effect, can be reduced to integrals over the azimuth angle as

$$\rho'_{mn} = \frac{1}{\sigma_m \sigma_n} \int_{-\pi}^{\pi} d\phi p(\phi) V_{rm}(\phi) V^*_{rn}(\phi) \tag{10}$$

with $1 \le m, n \le N_r$, $m \ne n$, and

$$\sigma_\ell^2 = \int_{-\pi}^{\pi} d\phi p(\phi) \left|V_{r\ell}(\phi)\right|^2.$$

With the direction-dependent coupling effects included, each component in (9) can be expressed as

$$V_{r\ell}(\phi) = \sum_{p=1}^{N_r} b_{\ell p} V_{\mathrm{oc}p}(\phi) + d_\ell(\phi).$$

Hence, the integral in (10) can be calculated as

$$\begin{aligned}
&\int_{-\pi}^{\pi} d\phi p(\phi) V_{rm}(\phi) V^*_{rn}(\phi) \\
&= \int_{-\pi}^{\pi} d\phi p(\phi) \left[\sum_{p=1}^{N_r} \sum_{q=1}^{N_r} b_{mp} b^*_{nq} V_{\mathrm{oc}p}(\phi) V^*_{\mathrm{oc}q}(\phi) \right. \\
&\qquad + d^*_n(\phi) \sum_{p=1}^{N_r} b_{mp} V_{\mathrm{oc}p}(\phi) \\
&\qquad \left. + d_m(\phi) \sum_{q=1}^{N_r} b^*_{nq} V^*_{\mathrm{oc}q}(\phi) + d_m(\phi) d^*_n(\phi) \right].
\end{aligned} \tag{11}$$

Similarly, σ_ℓ^2 can be calculated as

$$\begin{aligned}
\sigma_\ell^2 = \int_{-\pi}^{\pi} d\phi p(\phi) &\left[\sum_{p=1}^{N_r} \sum_{q=1}^{N_r} b_{\ell p} b^*_{\ell q} V_{\mathrm{oc}p}(\phi) V^*_{\mathrm{oc}q}(\phi) \right. \\
&+ d^*_\ell(\phi) \sum_{p=1}^{N_r} b_{\ell p} V_{\mathrm{oc}p}(\phi) + d_\ell(\phi) \sum_{q=1}^{N_r} b^*_{\ell q} V^*_{\mathrm{oc}q}(\phi) \\
&\left. + d_\ell(\phi) d^*_\ell(\phi) \right].
\end{aligned} \tag{12}$$

The covariance matrix $\bar{\bar{R}}'_t$ of the transmitting array, including the mutual coupling effect, can be calculated in the same manner. In other words, the receiving signals can be expressed as

$$\bar{y}' = \bar{\bar{C}}_r \cdot \bar{\bar{R}}'^{\frac{1}{2}}_r \cdot \bar{\bar{H}}_{\mathrm{i.i.d.}} \cdot \bar{\bar{R}}'^{\frac{1}{2}}_t \cdot \bar{\bar{C}}_t \cdot \bar{x} + \bar{n} = \bar{\bar{H}}'_c \cdot \bar{x} + \bar{n} \tag{13}$$

where the mutual coupling effects are included in the spatial correlation coefficients, as well as $\bar{\bar{C}}_t$ and $\bar{\bar{C}}_r$.

In (7), the receiving voltages $\bar{y}'$ are related to the transmitted signals $\bar{x}$ via $\bar{\bar{C}}_r \cdot \bar{\bar{H}} \cdot \bar{\bar{C}}_t$. When the correlation matrices of the transmitting and the receiving arrays are incorporated, the $\bar{\bar{H}}$ matrix is transformed to $\bar{\bar{R}}'^{1/2}_r \cdot \bar{\bar{H}}_{\mathrm{i.i.d.}} \cdot \bar{\bar{R}}'^{1/2}_t$, as shown in (13). Using the same notations as in (7), (9) can be rewritten as

$$\bar{y}' = \bar{\bar{B}} \cdot \bar{\bar{H}} \cdot \bar{\bar{C}}_t \cdot \bar{x} + \bar{D} + \bar{n} \tag{14}$$

where $\bar{V}_{\mathrm{oc}} = \bar{\bar{H}} \cdot \bar{\bar{C}}_t \cdot \bar{x}$, and the noise $\bar{n}$ is superposed at this stage. When the correlation matrices of the transmitting and the receiving arrays are incorporated, $\bar{\bar{H}}$ is transformed in the same way to $\bar{\bar{H}}' = \bar{\bar{R}}'^{1/2}_r \cdot \bar{\bar{H}}_{\mathrm{i.i.d.}} \cdot \bar{\bar{R}}'^{1/2}_t$; hence, (14) is transformed to

$$\bar{y}' = \bar{\bar{B}} \cdot \bar{\bar{H}}' \cdot \bar{\bar{C}}_t \cdot \bar{x} + \bar{D}(\phi) + \bar{n}. \tag{15}$$

The covariance matrix of $\bar{y}'$ can be derived as

$$\begin{aligned}
\bar{\bar{R}}'_{yy} = \mathrm{E}\left\{\bar{y}'\bar{y}'^{\dagger}\right\} &= \bar{\bar{B}} \cdot \bar{\bar{H}}' \cdot \bar{\bar{C}}_t \cdot \bar{\bar{R}}_{xx} \cdot \bar{\bar{C}}^{\dagger}_t \cdot \bar{\bar{H}}'^{\dagger} \cdot \bar{\bar{B}}^{\dagger} \\
&+ \bar{\bar{B}} \cdot \bar{\bar{H}}' \cdot \bar{\bar{C}}_t \cdot \mathrm{E}\{\bar{x}\bar{D}^{\dagger}\} + \mathrm{E}\{\bar{D}\bar{x}^{\dagger}\} \cdot \bar{\bar{C}}^{\dagger}_t \cdot \bar{\bar{H}}'^{\dagger} \cdot \bar{\bar{B}}^{\dagger} \\
&+ \bar{D}\bar{D}^{\dagger} + \sigma_n^2 \bar{\bar{I}}
\end{aligned}$$

where $\bar{x}$ and $\bar{D}$ are assumed uncorrelated to the noise $\bar{n}$.

Using the definition in (2), the average channel capacity can be expressed as

$$\begin{aligned}
C = &\max_{\bar{\bar{R}}_{xx}:\mathrm{Tr}\{\bar{\bar{R}}_{xx}\} \le P_t} \\
&\times \mathrm{E}\left\{ \log_2 \det \left[\bar{\bar{I}} + \frac{1}{\sigma_n^2} \left(\bar{\bar{B}} \cdot \bar{\bar{H}}' \cdot \bar{\bar{C}}_t \cdot \bar{\bar{R}}_{xx} \cdot \bar{\bar{C}}^{\dagger}_t \cdot \bar{\bar{H}}'^{\dagger} \cdot \bar{\bar{B}}^{\dagger} + \bar{\bar{B}} \cdot \bar{\bar{H}}' \right. \right. \right. \\
&\qquad \left. \left. \left. \cdot \bar{\bar{C}}_t \cdot \mathrm{E}\left\{\bar{x}\bar{D}^{\dagger}\right\} + \mathrm{E}\left\{\bar{D}\bar{x}^{\dagger}\right\} \right. \right. \right. \\
&\qquad \left. \left. \left. \cdot \bar{\bar{C}}^{\dagger}_t \cdot \bar{\bar{H}}'^{\dagger} \cdot \bar{\bar{B}}^{\dagger} + \bar{D}\bar{D}^{\dagger} \right) \right] \right\}.
\end{aligned} \tag{16}$$

IV. Capacity With Water-Filling Power Distribution Strategy

To calculate the channel capacity with the water-filling power distribution strategy, the transfer matrix $\bar{\bar{H}}'_c$ in (13), which includes the mutual coupling effect, is substituted into (2) to have

$$\begin{aligned}
C &= \max_{\bar{\bar{R}}_{xx}:\mathrm{Tr}\left\{\bar{\bar{R}}_{xx}\right\} \le P_t} \mathrm{E}\left\{ \log_2 \det \left[\bar{\bar{I}} + \frac{\bar{\bar{H}}'_c \cdot \bar{\bar{R}}_{xx} \cdot \bar{\bar{H}}'^{\dagger}_c}{\sigma_n^2} \right] \right\} \\
&= \max_{\bar{\bar{R}}'_{xx}:\mathrm{Tr}\left\{\bar{\bar{R}}'_{xx}\right\} \le P'_t} \mathrm{E}\left\{ \log_2 \det \left[\bar{\bar{I}} + \frac{1}{\sigma_n^2} \left(\bar{\bar{C}}_r \cdot \bar{\bar{H}}' \cdot \bar{\bar{R}}'_{xx} \cdot \bar{\bar{H}}'^{\dagger} \cdot \bar{\bar{C}}^{\dagger}_r \right) \right] \right\}
\end{aligned} \tag{17}$$

where $\bar{\bar{R}}'_{xx} = \bar{\bar{C}}_t \cdot \bar{\bar{R}}_{xx} \cdot \bar{\bar{C}}^{\dagger}_t$, $P'_t = P_t \mathrm{Tr}\{\bar{\bar{C}}_t \cdot \bar{\bar{C}}^{\dagger}_t\}/N_t$, and σ_n^2 is the average noise power at each receiving antenna.

Then, the optimal power P_m allocated to all the transmitting antennas is determined by applying the water-filling algorithm [19] to $\bar{\bar{R}}'_{xx}$

to achieve the channel capacity, i.e.,

$$C_{\mathrm{wf}} = \mathrm{E}\left\{\sum_{m=1}^{N_t} \log_2\left(1 + P_m \frac{\sigma_{p,m}^2}{\sigma_n^2}\right)\right\} \tag{18}$$

under the constraint that $\sum_{m=1}^{N_t} P_m \le P_t'$, where $\sigma_{p,m}$ are the singular values of $\bar{\bar{C}}_r \cdot \bar{\bar{H}}'$.

The transmitting power allocated to the mth antennas is $P_m = (1/\gamma_0 - 1/\gamma_m)^+$, where $\gamma_m = \sigma_{p,m}^2/\sigma_n^2$, and γ_0 is the cutoff value, which is determined from $\sum_{m=1}^{N_t} P_m = P_t'$, with $(a)^+ = a$ if $a > 0$ and $(a)^+ = 0$ if $a \le 0$.

V. Results and Discussions

In the subsequent simulations, we will consider a LOS link between the transmitting array and the receiving array of a MIMO system. Both arrays are composed of eight vertical half-wavelength dipoles, at a spacing of half wavelength and operating at 2.4 GHz. For the reason mentioned in Section III, we consider the scenarios with $\theta_{\mathrm{in}} = 90°$; hence, $P_v = 0$, and $\chi = 0$. Assume the receiving array is deployed along the x-axis, with its center at the origin. The azimuth angle of the broadside direction of the transmitting array is ϕ_0, which means $\phi_0 = 90°$ if these two arrays are placed face to face.

To begin with, consider a plane wave incident at $\phi = \phi_0$, with the PAS $p_\phi(\phi) = \delta(\phi - \phi_0)$. The channel capacity obtained with the strategy of uniformly distributed transmitting power can be calculated using (16), in which the covariance matrix is $\bar{\bar{R}}_{xx} = (P_t/N_t)\bar{\bar{I}}$, and the transmitted signals are $\bar{x} = \sqrt{P_t/N_t}[1, 1, \ldots, 1]^t$. The transmitted signals are uncorrelated to one another, and we set $P_t = 1$ (W) in the subsequent simulations.

Fig. 2(a) shows the channel capacity over an LOS link with $p(\phi) = \delta(\phi - \phi_0)$ and $\phi_0 = 15°$. The results are obtained by substituting the transfer functions $\bar{\bar{H}}_c'$, $\bar{\bar{H}}_c$, and $\bar{\bar{H}}$, respectively, into (5). The capacity predicted with (16) is also shown for comparison. The capacity based on the covariance matrices $\bar{\bar{R}}_t'$ and $\bar{\bar{R}}_r'$ in (13), which includes the mutual coupling effects, is higher than that based on the conventional covariance matrices $\bar{\bar{R}}_t$ and $\bar{\bar{R}}_r$ in (7). In other words, the mutual coupling effects tend to decrease the correlation coefficients, as defined in (10).

Fig. 2(b) shows the channel capacity, with the strategy of water-filling transmitting power. The results are obtained by substituting the transfer functions $\bar{\bar{H}}_c'$, $\bar{\bar{H}}_c$, and $\bar{\bar{H}}$, respectively, into (17). Compared with Fig. 2(a), it is observed that the water-filling strategy generally offers a higher capacity than the strategy of uniformly distributed transmitting power, particularly when $\bar{\bar{H}}_c'$ and $\bar{\bar{H}}_c$ are used. For example, the capacity increase from 2 to 3 bits/s/Hz at SNR $= 20$ dB. The capacity using $\bar{\bar{H}}$ in (4) is higher than that of the other coupling assumptions, with either transmitting power strategy.

Fig. 3 shows the channel capacity of an 8×8 MIMO system, with $\phi_0 = 90°$, using the strategy of uniformly distributed transmitting power. At high SNR values, the capacity using (16) or $\bar{\bar{H}}_c'$ in (13) is higher than that using $\bar{\bar{H}}$ in (4).

With the strategy of water-filling transmitting power, the capacity using $\bar{\bar{H}}_c'$ in (13) is higher than that using $\bar{\bar{H}}$ in (4). At SNR $= 20$ dB, the capacity using the water-filling strategy is higher than that using the uniformly distributed strategy by about 3 bits/s/Hz.

In the matrix $\bar{\bar{H}}$ of (4), no coupling effects among antennas are considered, and the correlation coefficients without coupling effects are used. In the matrix $\bar{\bar{H}}_c$ of (7), the coupling effects among antennas are considered, and the same correlation coefficients without coupling effects are used. In matrix $\bar{\bar{H}}_c'$ of (13), both the coupling effects among antennas and the correlation coefficients with coupling effects are included.

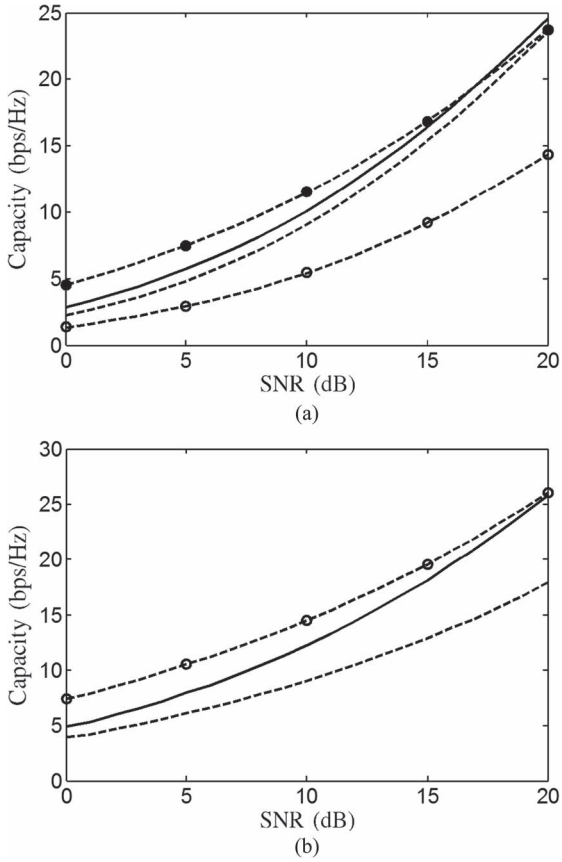

Fig. 2. Capacity of an 8×8 MIMO system over an LOS channel with $p(\phi) = \delta(\phi - \phi_0)$ and $\phi_0 = 15°$, 1000 Monte-Carlo channel realizations at each SNR. (a) Strategy of uniformly distributed transmitting power: ———: using (16); $- - -$: using $\bar{\bar{H}}_c'$ in (13); $- \circ -$: using $\bar{\bar{H}}_c$ in (7); $- \bullet -$: using $\bar{\bar{H}}$ in (4). (b) Strategy of water-filling transmitting power: ———: using $\bar{\bar{H}}_c'$ in (13); $- - -$: using $\bar{\bar{H}}_c$ in (7); $- \circ -$: using $\bar{\bar{H}}$ in (4).

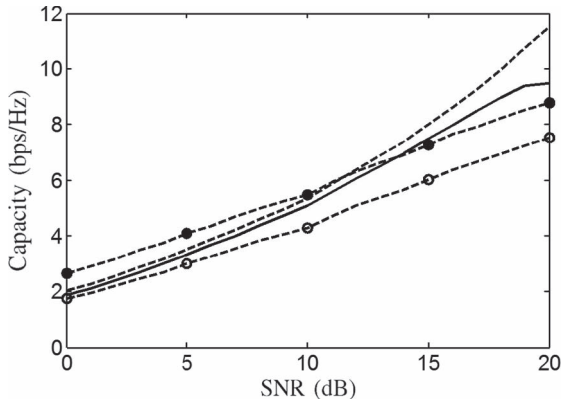

Fig. 3. Capacity of an 8×8 MIMO system over an LOS channel with the same parameters as in Fig. 2, except $\phi_0 = 90°$. Strategy of uniformly distributed transmitting power: ———: using (16); $- - -$: using $\bar{\bar{H}}_c'$ in (13); $- \circ -$: using $\bar{\bar{H}}_c$ in (7); $- \bullet -$: using $\bar{\bar{H}}$ in (4).

In Fig. 3, the transmitting array is placed face-to-face with the receiving array ($\phi_0 = 90°$). The correlation coefficients calculated using (10) become close to one; hence, the channel capacities decrease significantly as compared with their counterparts in Fig. 2(a) and (b). Under such circumstances, by including the subtle difference attributed to the mutual coupling among antennas in both arrays and the coupling effects in the correlation coefficients, as in $\bar{\bar{H}}_c'$, the capacity can

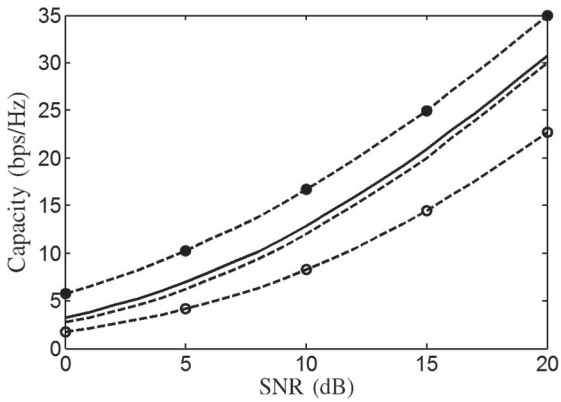

Fig. 4. Capacity of an 8 × 8 MIMO system over a channel with single-cluster Laplacian PAS, $\phi_0 = 90^\circ$, $\phi_1 = 15^\circ$, $\sigma_L = 30^\circ$, and $\Delta\phi = 60^\circ$; 1000 Monte Carlo channel realizations at each SNR. Strategy of uniformly distributed transmitting power: ———: using (16); − − −: using $\bar{\bar{H}}_c'$ in (13); − ∘ −: using $\bar{\bar{H}}_c$ in (7); − • −: using $\bar{\bar{H}}$ in (4).

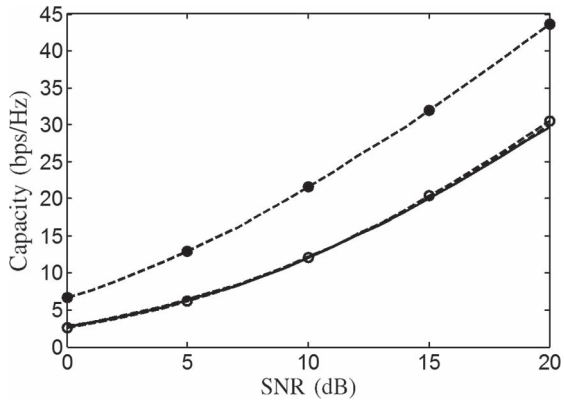

Fig. 5. Capacity of an 8 × 8 MIMO system over a channel with single-cluster Laplacian PAS, $\phi_0 = 90^\circ$, $\phi_1 = 90^\circ$, $\sigma_L = 45^\circ$, and $\Delta\phi = 90^\circ$; 1000 Monte Carlo channel realizations at each SNR. (a) Strategy of uniformly distributed transmitting power: ———: using (16); − − −: using $\bar{\bar{H}}_c'$ in (13); − ∘ −: using $\bar{\bar{H}}_c$ in (7); and − • −: using $\bar{\bar{H}}$ in (4).

be increased higher than that using $\bar{\bar{H}}$ at high SNR values. Such a capacity increase is significant to many LOS MIMO applications with $\phi_0 \simeq 90^\circ$.

The PAS in the azimuthal plane can be characterized with a Laplacian PAS in both polarizations [20]. In the subsequent simulations, we will use a truncated multicluster Laplacian PAS [7]

$$p_L(\phi) = \sum_{\ell=1}^{N_c} \frac{Q_{L,\ell}}{\sigma_{L,\ell}\sqrt{2}} e^{-\sqrt{2}|\phi-\phi_\ell|/\sigma_{L,\ell}} \times \{u[\phi - (\phi_\ell - \Delta\phi_\ell)] - u[\phi - (\phi_\ell + \Delta\phi_\ell)]\}$$

where $u(\phi)$ is the step function, N_c is the number of clusters, ϕ_ℓ is the direction of arrival from the ℓth cluster covering the azimuthal interval of $[\phi_\ell - \Delta\phi_\ell, \phi_\ell + \Delta\phi_\ell]$, σ_L is the standard deviation of the PAS that accounts for the angular spread, and $Q_{L,\ell}$ is a normalization factor to make $p_L(\phi)$ a probability density function, namely, $\sum_{\ell=1}^{N_c} Q_{L,\ell}[1 - e^{-\sqrt{2}\Delta\phi_\ell/\sigma_{L,\ell}}] = 1$.

Fig. 4 shows the capacity of an 8 × 8 MIMO system in the presence of a single-cluster Laplacian PAS, with the strategy of uniformly distributed transmitting power. The capacity using $\bar{\bar{H}}_c'$ in (13) is higher than that using $\bar{\bar{H}}_c$ in (7). Since the transfer matrix $\bar{\bar{H}}_c'$ includes the mutual coupling effects in determining the covariance matrices, leading to smaller correlation coefficients and hence higher capacity. The capacity using (16) is higher than that using $\bar{\bar{H}}_c'$ in (13) because the mutual coupling effects at different incident angles have been taken into account.

If the strategy of water-filling transmitting power is applied to the same MIMO system in the presence of the same single-cluster Laplacian PAS, the capacity calculated using $\bar{\bar{H}}_c'$ in (13) is higher than that using $\bar{\bar{H}}_c$ in (7). The capacities are higher than their counterparts obtained by applying the uniformly distributed strategy.

The truncated Laplacian PAS has a finite angular spread σ_L, making the correlation coefficients smaller than those associated with a LOS channel. Hence, the capacities shown in Fig. 4 are higher than their counterparts in Figs. 2 and 3.

The capacity using $\bar{\bar{H}}$ in (4) is higher than that using other coupling assumptions, with either transmitting power strategy. The multipath signals characterized with the single-cluster Laplacian PAS appear to dominate over the mutual coupling effects among antennas in both the transmitting and the receiving arrays. At SNR = 20 dB, the capacity using the water-filling strategy is higher than that using the uniformly distributed strategy by about 1 to 2.5 bits/s/Hz.

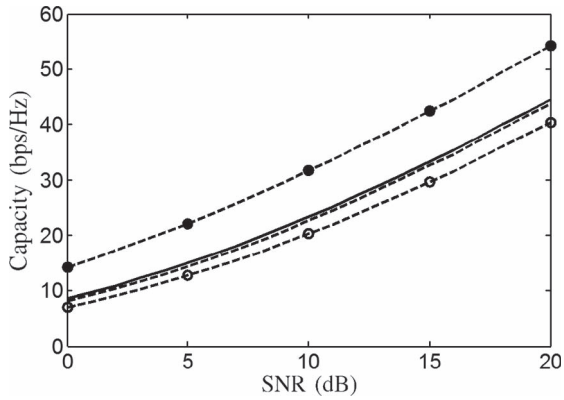

Fig. 6. Capacity of an 8 × 8 MIMO system over a channel with two equal-power clusters of Laplacian PAS, $\phi_0 = 90^\circ$, $\phi_1 = 30^\circ$, $\sigma_{L1} = 10^\circ$, $\Delta\phi_1 = 20^\circ$, $\phi_2 = 90^\circ$, $\sigma_{L2} = 10^\circ$ and $\Delta\phi_2 = 20^\circ$; 1000 Monte-Carlo channel realizations at each SNR. (a) Strategy of uniformly distributed transmitting power: ———: using (16); − − −: using $\bar{\bar{H}}_c'$ in (13); − ∘ −: using $\bar{\bar{H}}_c$ in (7); − • −: using $\bar{\bar{H}}$ in (4).

Fig. 5 shows the capacity of an 8 × 8 MIMO system with the uniformly distributed transmitting power strategy. Similar to the results shown in Fig. 4, the capacities calculated using (16), $\bar{\bar{H}}_c'$ in (13), and $\bar{\bar{H}}_c$ in (7) are smaller than that using $\bar{\bar{H}}$ in (4). The same trend is observed if the water-filling transmitting power strategy is applied.

The angular spread σ_L and the angular coverage $\Delta\phi$ used in Fig. 5 are larger than those used in Fig. 4. The capacities calculated using $\bar{\bar{H}}_c'$ in (13) and $\bar{\bar{H}}_c$ in (7) are almost the same, and the capacities with both transmitting power strategies are also very close. At SNR = 20 dB, the capacities using $\bar{\bar{H}}$ in (4) are higher than their counterparts shown in Fig. 4 by about 10 bits/s/Hz, which is attributed to larger σ_L and $\Delta\phi$.

Fig. 6 shows the capacity of an 8 × 8 MIMO system with uniformly distributed transmitting power strategy, under two clusters of Laplacian PAS with equal power. The capacities with a water-filling strategy are very close to those shown in Fig. 6. However, unlike the results shown in Fig. 5, the capacity calculated using $\bar{\bar{H}}_c'$ in (13) is higher than that using $\bar{\bar{H}}_c$ in (7) because the angular spread σ_L and the angular coverage $\Delta\phi$ used in Fig. 6 are smaller than those used in Fig. 5. With two clusters of Laplacian PAS, the capacity at SNR = 20 dB is about 10 bits/s/Hz higher than that in Fig. 5 possibly because more multipath signals appear between the transmitting and the receiving arrays.

VI. Conclusion

The reciprocity theorem is applied to derive an exact expression that is used to remove the coupling effects embedded in the receiving voltages of an antenna array. The correlation coefficients of the multiple-input–multiple-output (MIMO) channel established with the antenna array is also modified to incorporate the direction-dependent coupling effects more accurately. The simulation results show that, in propagation environments dominated by a LOS signal, the capacity of a MIMO channel can be increased by properly incorporating the coupling effects. The mutual coupling effects can be neglected in environments dominated by multipath signals, where the capacity is determined by the PAS characterizing the channel.

References

[1] G. J. Foschini and M. J. Gans, "On limits of wireless communications in a fading environment when using multiple antennas," *Wireless Pers. Commun.*, vol. 6, no. 3, pp. 311–335, Mar. 1998.

[2] T. K. Sarkar, M. Salazar-Palma, and E. L. Mokole, *Physics of Multiantenna Systems and Broadband Processing*. Hoboken, NJ, USA: Wiley, 2008.

[3] R. Janaswamy, "Effect of element mutual1 coupling on the capacity of fixed length linear arrays," *Antennas Wireless Propag. Lett.*, vol. 1, no. 1, pp. 157–160, 2002.

[4] T. Svantesson and A. Ranheim, "Mutual coupling effects on the capacity of multielement antenna systems," in *Proc. IEEE ICASSP*, vol. 4, pp. 2485–2488, May 2001.

[5] J. W. Wallace and M. A. Jensen, "Mutual coupling in MIMO wireless systems: A rigorous network theory analysis," *IEEE Trans. Wireless Commun.*, vol. 3, pp. 1317–1325, Jul. 2004.

[6] R. G. Vaughan and J. B. Andersen, "Antenna diversity in mobile communications," *IEEE Trans. Veh. Technol.*, vol. VT-36, no. 4, pp. 149–172, Nov. 1987.

[7] L. Schumacher, K. I. Pedersen, and P. E. Mogensen, "From antenna spacings to theoretical capacities-Guidelines for simulating MIMO systems," in *Proc. IEEE Int. Symp. PIMRC*, 2002, vol. 2, pp. 587–592.

[8] C. Waldschmidt and W. Wiesbeck, "Compact wide-band multimode antennas for MIMO and diversity," *IEEE Trans. Antennas Propag.*, vol. 52, no. 8, pp. 1963–1969, Aug. 2004.

[9] A. Capobianco *et al.*, "A compact MIMO array of planar end-fire antennas for WLAN applications," *IEEE Trans. Antennas Propag.*, vol. 59, no. 9, pp. 3462–3465, Sep. 2011.

[10] Z. Y. Li, Z. W. Du, M. Takahashi, K. Saito, and K. Ito, "Reducing mutual coupling of MIMO antennas with parasitic elements for mobile terminals," *IEEE Trans. Antennas Propag.*, vol. 60, no. 2, pp. 473–481, Feb. 2012.

[11] M. A. Jensen and J. W. Wallace, "A review of antennas and propagation for MIMO wireless communications," *IEEE Trans. Antennas Propag.*, vol. 52, no. 11, pp. 2810–2824, Nov. 2004.

[12] W. C. Jakes, *Microwave Mobile Communications*. Piscataway, NJ, USA: IEEE Press, 1993.

[13] D. Chizhik *et al.*, "Multiple-input-multiple-output measurements and modeling in Manhattan," *IEEE J. Sel. Areas Commun.*, vol. 21, no. 3, pp. 321–331, Apr. 2003.

[14] E. A. Jorswieck and H. Boche, "Channel capacity and capacity-range of beamforming in MIMO wireless systems under correlated fading with covariance feedback," *IEEE Trans. Wireless Commun.*, vol. 3, no. 5, pp. 1543–1553, Sep. 2004.

[15] D. W. Browne, M. Manteghi, M. P. Fitz, and Y. Rahmat-Samii, "Experiments with compact antenna arrays for MIMO radio communications," *IEEE Trans. Antennas Propag.*, vol. 54, no. 11, pp. 3239–3250, Nov. 2006.

[16] S. Durrani and M. E. Bialkowski, "Effect of mutual coupling on the interference rejection capabilities of linear and circular arrays in CDMA systems," *IEEE Trans. Antennas Propag.*, vol. 52, no. 4, pp. 1130–1134, Apr. 2004.

[17] B. Clerckx, C. Craeye, D. Vanhoenacker-Janvier, and C. Oestges, "Impact of antenna coupling on 2×2 MIMO communications," *IEEE Trans. Veh. Technol.*, vol. 56, no. 3, pp. 1009–1018, May 2007.

[18] K. R. Dandekar, H. Ling, and G. Xu, "Experimental study of mutual coupling compensation in smart antenna applications," *IEEE Trans. Wireless Commun.*, vol. 1, no. 3, pp. 480–487, Jul. 2002.

[19] M. A. Khalighi, J. Brossier, G. Jourdain, and K. Raoof, "Water filling capacity of Rayleigh MIMO channels," in *Proc. IEEE Int. Symp. PIMRC*, San Diego, CA, USA, Sep./Oct. 2001, vol. 1, pp. 155–158.

[20] Q. H. Spencer, B. D. Jeffs, M. A. Jensen, and A. L. Swindlehurst, "Modeling the statistical time and angle of arrival characteristics of an indoor multipath channel," *IEEE J. Sel. Areas Commun.*, vol. 18, no. 3, pp. 347–360, Mar. 2000.

On the Capacity of Joint Fading and Two-Path Shadowing Channels

I. Dey, *Student Member, IEEE*, G. G. Messier, *Member, IEEE*, and S. Magierowski, *Member, IEEE*

***Abstract*—The ergodic and outage channel capacity of different optimal and suboptimal combinations of transmit power and modulation rate adaptation strategies over a joint fading and two-path shadowing (JFTS) fading/shadowing channel is studied in this paper. Analytically tractable expressions for channel capacity are obtained, assuming perfect channel side information (CSI) at the receiver and/or the transmitter with negligible feedback delay. Furthermore, the impacts of the JFTS parameters on the channel capacity achieved by these adaptive transmission techniques are determined.**

***Index Terms*—Adaptive transmission, channel capacity, fading, shadowing.**

I. Introduction

The high density and considerable individual data rate requirements of modern indoor wireless users have made high-capacity wireless communications a priority in indoor environments. While the use of indoor picocells is expected to grow, this demand is primarily being served today by indoor wireless access points. Therefore, it is essential to have an accurate picture of what high-throughput wireless communication systems can achieve when implemented on densely deployed indoor access points.

This picture is provided by Shannon channel capacity. With the introduction of capacity-achieving coding schemes [3], Shannon capacity is now of both theoretical and practical interest. In the case of wireless links, Shannon channel capacity characterizes the long-term achievable information rate and is, therefore, called the ergodic capacity [1].

In a fading environment, the Shannon bound can be achieved by adapting a variety of parameters relative to the channel quality if perfect channel side information (CSI) is available at the receiver and/or the transmitter [5]–[7]. Examples include optimal rate adaptation (ORA) [8], which adapts modulation constellation size, and optimal power and rate adaptation (OPRA) [7], which adapts a combination of modulation rate and transmit power. The Shannon capacity can be also achieved only through optimal power control by using fading inversion to maintain a constant carrier signal-to-noise ratio (CSNR). This technique is known as channel inversion with fixed rate (CIFR) [7], [8].

Manuscript received June 26, 2014; revised November 15, 2014; accepted January 9, 2015. Date of publication January 21, 2015; date of current version January 13, 2016. The review of this paper was coordinated by Prof. H.-F. Lu.

I. Dey and G. G. Messier are with the Department of Electrical and Computer Engineering, University of Calgary, Calgary, AB T2N 1N4, Canada (e-mail: deyi@ucalgary.ca; gmessier@ucalgary.ca).

S. Magierowski is with the Department of Electrical Engineering and Computer Science, Lassonde School of Engineering, York University, Toronto, ON M3J 1P3, Canada (e-mail: magiero@cse.yorku.ca).

Digital Object Identifier 10.1109/TVT.2015.2394372